

# The Weight of a Bit: EMFI Sensitivity Analysis of Embedded Deep Learning Models

Jakub Breier, Štefan Kučerák, Xiaolu Hou

**Abstract**—Fault injection attacks on embedded neural network models have been shown as a potent threat. Numerous works studied resilience of models from various points of view. As of now, there is no comprehensive study that would evaluate the influence of number representations used for model parameters against electromagnetic fault injection (EMFI) attacks.

In this paper, we investigate how four different number representations influence the success of an EMFI attack on embedded neural network models. We chose two common floating-point representations (32-bit, and 16-bit), and two integer representations (8-bit, and 4-bit). We deployed four common image classifiers, ResNet-18, ResNet-34, ResNet-50, and VGG-11, on an embedded memory chip, and utilized a low-cost EMFI platform to trigger faults. Our results show that while floating-point representations exhibit almost a complete degradation in accuracy (Top-1 and Top-5) after a single fault injection, integer representations offer better resistance overall. Especially, when considering the the 8-bit representation on a relatively large network (VGG-11), the Top-1 accuracies stay at around 70% and the Top-5 at around 90%.

**Index Terms**—Neural networks, electromagnetic fault injection, neural network security

## I. INTRODUCTION

EMBEDDED implementations of neural networks are gaining popularity with frameworks such as TinyML [1], allowing a real-time, efficient execution in the Edge. The applications range from the Internet of Things to mobile devices to autonomous systems, offering significant benefits: reduction in latency, improved data privacy, removing the necessity of a constant network connection, to name a few. These lightweight frameworks take pre-trained models and optimize them with various techniques, such as quantization and pruning [2], to fit in the resource-constrained hardware. The result is the ability of small microcontrollers with only a few kilobytes of RAM to run models for image classification, anomaly detection, and others, effectively moving away from the classical cloud setup.

This naturally introduces new security and reliability challenges due to malicious and environmental influences stemming from the physical accessibility of these devices. Fault injection attacks (FIAs) are one notable threat where the attacker disturbs the operation of the device to introduce errors,

J. Breier is with TTControl GmbH, Vienna, Austria. E-mail: jbreier@jbreier.com.

Š. Kučerák and X. Hou are with the Faculty of Informatics and Information Technologies, Slovak University of Technology, Slovakia. X. Hou is also affiliated with the State Key Laboratory of Blockchain and Data Security, Zhejiang University. E-mail: xkucera@stuba.sk, houxiaolu.email@gmail.com.

This work was supported by the Open Research Fund of The State Key Laboratory of Blockchain and Data Security, Zhejiang University under grant no. A2566.

either in the data or execution flow [3]. Electromagnetic fault injection (EMFI) [4] is a fault injection technique that is non-invasive and does not need a sophisticated, expensive device to perform. The attacker uses a high-power pulse generator to inject a sharp electromagnetic pulse, introducing transient faults in the device’s electronic circuits. These faults can either cause bit flips in the memory or skip the instructions being executed, resulting in the misbehavior of the neural network model, as shown in [5].

When deploying neural networks on a microcontroller, one needs to consider the numerical representation of model parameters. To achieve memory and power savings, it is standard to use reduced-precision formats: for instance, 32-bit floating-point weights can be reduced to 16-bit floats, 8-bit integers, and in extreme cases even to 4-bit or binary weights [6]. While such precision reduction/quantization introduces an approximation error, when used properly, a quantized model can retain almost the same accuracy as the original one [7]. At the same time, quantization changes the fault tolerance characteristics of a network, leading to different vulnerability profiles under fault injection [8]. Intuitively, a bit flip in an integer weight has a bounded effect, especially since the weight range is limited by the quantization scale, whereas in a floating-point weight, an upset in the exponent bit can have a significant influence on the network’s output, as was investigated in [9]. In integer formats, the most significant bits are the critical ones for a network’s computation, while in floating-point, the exponent and higher-order mantissa bits carry the most significance. Furthermore, larger models provide inherent redundancy that compensate for some faults.

The open question, and the main focus of this paper, is how these factors play out in practice:

*To what extent does the choice of weight number format (from high-precision to aggressively quantized) influence a neural network’s resilience against EMFI attacks?*

Despite growing awareness of both quantization techniques and fault injection threats, this specific question remains only partially answered by prior research. Most existing studies of neural network fault tolerance have considered a single representation (often full 32-bit precision, or a very low-bit scheme in isolation), rather than comparing formats, thus a systematic investigation is warranted [8], [10].

**Our contribution.** In this work, we conduct an extensive empirical study to quantitatively evaluate the influence of weight number format on the fault injection resilience of neural networks. We consider four widely-used numeric formats for weights: 32-bit float (FP32), 16-bit float (FP16),

8-bit integer (INT8), and 4-bit integer (INT4), covering the spectrum from full precision to highly quantized. To probe their fault tolerance, we select several representative convolutional neural network (CNN) models (ResNet-18, ResNet-34, ResNet-50 [11], and VGG-11 [12]) trained on the ImageNet-1K dataset [13] and implement each model in all four formats on an embedded inference platform. We then subject these networks to experimental EMFI attack campaigns using a NewAE ChipSHOUTER platform. By injecting electromagnetic glitches during the models' inference and observing the resulting behavior, we measure how often and how severely each attack disrupts the model's accuracy. This methodology allows us to directly compare the robustness of different weight representations under identical attack conditions. Our study reveals notable differences: certain models and formats show graceful degradation under faults, while others suffer immediate and sharp accuracy drops even for small amount of faults. To our knowledge, this is the first comparative analysis of a deep neural network (DNN) fault injection robustness across multiple weight precisions.

**Organization.** The rest of the paper is organized as follows. Section II overviews a related work in the field and Section III gives the necessary background. Evaluation method on an experimental hardware is described in Section IV, followed by Section V that details the results of this work. Section VI provides the discussion, and finally, Section VII concludes this paper and provides directions for future work.

## II. RELATED WORK

A number of prior works have begun to explore the intersection of neural network quantization/representation and fault attacks, which we briefly review here and summarize in Table I.

One of the first attacks showed that by selecting and flipping a specific bit in a 32-bit floating point representation, it is possible to reduce the network accuracy by  $\approx 90\%$  [9].

In the domain of fault attacks on quantized neural networks, one of the earliest studies showed that by strategically flipping a few weight bits (via a Rowhammer-induced memory fault), an attacker could force a DNN classifier into misclassifying virtually all inputs, effectively reducing its accuracy to nearly random guess [14]. Along with the previous work, this demonstrated the outsized impact that even low-level data corruption can have on network accuracy, whether it is represented in a floating-point or an integer format.

SNIFF method [15] took fault attacks further by using them for model extraction: it allowed to reverse-engineer the parameters of a neural network by inducing sign-bit flips in the network's computations. By using high-precision arithmetic in their experiments, the authors were able to recover model weights with negligible error (on the order of  $10^{-13}$ ), essentially stealing a proprietary model with far fewer queries than a standard black-box approach.

On the other hand, research in neural network reliability has looked at how model design choices (like quantization) affect tolerance to unintentional faults (for example, soft errors or radiation-induced bit flips). In [16], the authors investigated CNNs on FPGAs under radiation-induced single-event upsets, comparing a baseline full-precision model to a binarized (1-bit weights) model. They found that the quantized (binary) network was about 39% less sensitive to radiation-induced faults than the full-precision network, presumably because the simpler binary representation and reduced parameter count offered a smaller attack surface in terms of bits that can be flipped. However, they also observed a trade-off: the fraction of faults that led to output misclassification was slightly higher (by  $\approx 12\%$ ) in the binary network, indicating that while fewer faults occurred, those that did were somewhat more likely to cause an error in inference.

In another recent study [8], the authors examined the fault tolerance of quantized and pruned CNN models. They developed a statistical fault injection framework (SFI4NN) to efficiently evaluate large networks, and reported that as networks are more aggressively pruned (sparser), their sensitivity to bit flips increases, presumably due to less redundancy in the parameters. To counter this, they proposed a selective redundancy mechanism (a lightweight error mitigation technique) and demonstrated it could improve a quantized CNN's resilience by about 96% compared to an unprotected model.

On the hardware side, [17] recently demonstrated practical EMFI and laser fault attacks on a microcontroller running an 8-bit quantized CNN. They showed that even a single instruction skip fault (induced by an EM pulse or laser shot) during a forward pass can alter the network's prediction or cause a persistent "memory effect" in the computations, highlighting the real-world feasibility of such attacks on TinyML devices.

Another closely related work [10] specifically looked at EMFI on a TinyML hardware platform with INT8 weight storage. They found that small, lightweight models suffered major accuracy degradation under EMFI, whereas larger mod-

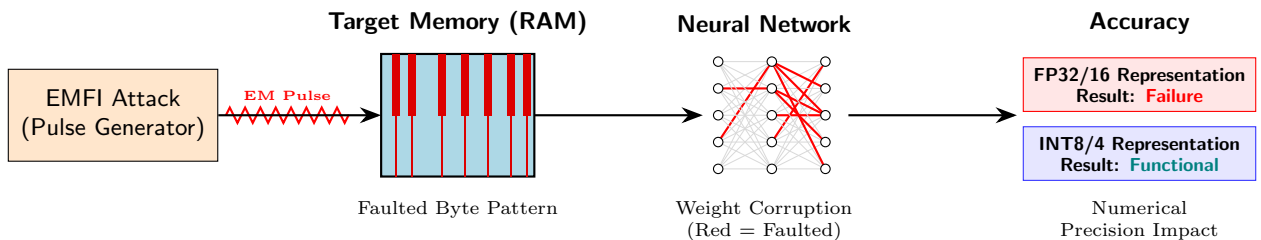


Fig. 1. Overview of the EMFI analysis done in this paper.

TABLE I  
SUMMARY OF RELATED WORK ON FAULT INJECTION ON NEURAL NETWORK REPRESENTATIONS.

Prior work	Attack type	Target model & platform	Weight format	Main findings
Hong <i>et al.</i> [9]	Bit-flip attack (memory fault via Rowhammer)	19 Deep CNN classifiers; simulated attack	32-bit floating point	Flipping a specific single bit can cause an accuracy loss of over 90%.
Rakin <i>et al.</i> [14]	Bit-flip attack (memory fault via Rowhammer)	Deep CNN classifiers; simulated attack	8/6/4-bit integer	Flipping $\sim 13$ weight bits can degrade a network's accuracy to $\sim 0\%$ (misclassification of virtually all inputs).
Breier <i>et al.</i> [15]	Fault injection for model extraction (sign-bit flips)	Deep feature-extractor network; simulated attack	32/64-bit floating point	By flipping sign bits of activations, achieved $< 10^{-13}$ error in recovered weights, effectively stealing the DNN model.
Libano <i>et al.</i> [16]	Radiation-induced soft errors (fault injection & accelerated radiation tests)	Small CNN on FPGA (MNIST digit recognition)	1-bit binary vs. 32-bit float	Binary-weight network showed 39% fewer erroneous outputs under faults, but 12% more of its errors were catastrophic (misclassifications) compared to full-precision.
Guillemé <i>et al.</i> [8]	Statistical fault injection (simulated bit flips)	AlexNet-like CNN, software simulation; evaluated pruning and quantisation	8-bit integer (with varying pruning levels)	Pruning increases fault sensitivity (less redundancy). Proposed selective redundancy (hardware voting) improved fault tolerance by $\sim 96\%$ vs. no protection.
Gaine <i>et al.</i> [17]	Electromagnetic & laser fault injection (instruction skip)	CNN (2-layer ConvNet) on ARM Cortex-M4 microcontroller (embedded device)	8-bit integer (CMSIS-NN quantized)	First demonstrated EMFI/LFI on a real CNN inference: single-glitch instruction skips in convolution or activation routines caused targeted mispredictions and persistent erroneous states.
Goswami <i>et al.</i> [10]	Electromagnetic fault injection (transient bit flips in NVM)	TinyML hardware platform with FRAM storage; models: MobileNet, ResNet, EfficientNet on CIFAR-10	8-bit integer	EM pulses during weight loading corrupted stored weights, leading to up to 40% accuracy loss in lightweight models (larger models fared better due to higher redundancy).
<b>This work</b>	Electromagnetic fault injection (transient bit flips in NVM)	Embedded memory chip hosting model parameters of ResNet-18, ResNet-34, ResNet-50, VGG-11	32/16-bit floating point, 8/4-bit integer	Floating point representations degrade significantly in accuracy, while integer ones offer more resistance to faults, especially for larger networks. The best trade-off is offered by the 8-bit integer quantization.

els with more parameters (and presumably more redundancy) were somewhat more robust.

In summary, these related studies show a growing awareness of the security implications of neural network representations. None of the existing works, however, provides a direct head-to-head comparison of different numeric formats under the same fault injection conditions and with the same models – the gap that our paper aims to fill. By comparing FP32, FP16, INT8, and INT4 in a unified experimental setup, our work builds upon the above research to provide new insights into how model precision and fault resilience are connected.

### III. BACKGROUND

In this section, we first provide an overview of embedded neural network implementations in Subsection III-A. Then, we detail the number formats used for weight representations studied in this work in Subsection III-B. Afterwards, we discuss different attack goals of FIAs on neural network implementations (Subsection III-C), and the physics behind electromagnetic fault injection (Subsection III-D).

#### A. Embedded and Edge Neural Network Implementations

The deployment of deep learning models on edge devices, often referred to as Edge AI or TinyML [18], represents a paradigm shift from centralized cloud-based training to on-device inference. This shift is driven by the requirement for low latency, data privacy, and reduced bandwidth consumption. However, embedded targets, ranging from constrained microcontrollers (MCUs) to embedded GPUs, operate under strict power and memory budgets. This necessitates the use of specialized software frameworks designed to execute the numerical representations described in the Subsection III-B.

1) *TinyML and Resource Constraints:* TinyML specifically targets the most constrained class of devices, typically running on microcontrollers (e.g., ARM Cortex-M) with limited SRAM and flash memory, often operating in the milliwatt power range. Unlike server-grade deployments, these implementations cannot rely on massive parallelization or virtually infinite memory. Consequently, models must be aggressively compressed and optimized before deployment. In this context, the physical integrity of memory is paramount; investigating fault injection in TinyML is critical because the redundancy

typically found in large, over-parameterized cloud models is often removed during the optimization process.

2) *TensorFlow Lite (TFLite)*: TensorFlow Lite [19] is a widely adopted open-source framework designed for on-device inference. The deployment workflow involves converting a trained model into the efficient FlatBuffer-based `.tflite` format using the TFLite Converter. This conversion process performs several graph optimizations essential for embedded execution:

- **Operator fusion:** combining multiple operations (e.g., convolution followed by an activation function) into a single computational kernel to reduce memory access overhead.
- **Quantization-aware conversion:** transforming weights from FP32 to INT8 or INT4, allowing the model to run on integer-only arithmetic logic units (ALUs) common in low-power MCUs.

The TFLite Interpreter then executes this optimized graph. Because TFLite relies on static memory planning to minimize runtime allocation, it presents a deterministic target for electromagnetic fault injection attacks.

### B. Number Formats

We used two floating-point representations and two integer representations for our study (see Table II for the summary). In this part, we explain each representation in detail, more information can be found, for example, in [20].

1) *Floating-Point Representations*: Floating-point arithmetic allows for a wide dynamic range, making it the standard for training deep learning models. These formats follow the IEEE 754 standard, dividing the binary representation into three components: the sign bit ( $s$ ), the biased exponent ( $e$ ), and the fraction or mantissa ( $m$ ).

a) *Single Precision (FP32)*: FP32 is the standard format for training neural networks on general-purpose GPUs and CPUs. It occupies 32 bits allocated as follows: 1 sign bit, 8 exponent bits, and 23 mantissa bits. The value  $v$  of an FP32 number is calculated using Equation (1), where the exponent bias is 127:

$$v_{FP32} = (-1)^s \times 2^{e-127} \times (1.m) \quad (1)$$

This format provides a high dynamic range (approximately  $\pm 3.4 \times 10^{38}$ ) and high precision, making it resilient to vanishing gradients during training but memory-intensive for inference on embedded targets.

b) *Half Precision (FP16)*: To reduce memory bandwidth and storage requirements, FP16 compresses the representation into 16 bits: 1 sign bit, 5 exponent bits, and 10 mantissa bits. The value is derived using an exponent bias of 15:

$$v_{FP16} = (-1)^s \times 2^{e-15} \times (1.m) \quad (2)$$

While FP16 halves the memory footprint compared to FP32, the reduced exponent width significantly shrinks the dynamic range (approximately  $\pm 6.5 \times 10^4$ ). This makes the model more sensitive to numerical instability, though it is often sufficient for inference in many embedded applications.

2) *Quantized Integer Representations*: Quantization maps continuous floating-point values to a discrete set of low-precision integers. This is critical for embedded inference, as integer arithmetic units are generally faster and more energy-efficient than floating-point units. In uniform affine quantization, a real floating-point value  $r$  is mapped to a quantized integer  $q$  using a scale factor  $S$  and a zero-point  $Z$ :

$$q = \text{round}\left(\frac{r}{S}\right) + Z \quad (3)$$

a) *8-bit Integer (INT8)*: INT8 is the prevalent quantization standard for edge AI inference (e.g., TensorFlow Lite, TensorRT). It utilizes 8 bits to represent signed integers, typically using two's complement notation, resulting in a range of  $[-128, 127]$ . INT8 reduces the model size by a factor of 4 compared to FP32. Due to its limited dynamic range of 256 discrete levels, INT8 typically relies on uniform affine quantization, where floating-point weights are mapped to integers using calibrated quantization parameters  $S$  and  $Z$  to minimize accuracy degradation.

b) *4-bit Integer (INT4)*: INT4 represents an aggressive low-bit-width number format used in extreme edge scenarios or for compressing large language models (LLMs). It utilizes only 4 bits per weight, providing an 8 $\times$  compression ratio over FP32, with a signed two's complement range of  $[-8, 7]$ . However, the coarseness of having only 16 representable values makes this format highly sensitive to perturbations. In the context of fault injection, a single bit flip in an INT4-encoded weight can induce a large relative change in its numerical value, corresponding to a substantial fraction of the total dynamic range.

TABLE II  
SUMMARY OF DATA REPRESENTATIONS.

Format	Total bits	Range	Decimal digits
FP32	32	$\pm 3.4 \times 10^{38}$	$\sim 7$
FP16	16	$\pm 6.55 \times 10^4$	$\sim 3\text{--}4$
INT8	8	$[-128, 127]$	Exact
INT4	4	$[-8, 7]$	Exact

### C. Fault Injection Attacks on Neural Networks

Fault injection attacks (FIA) were originally proposed as an active hardware attack method on cryptosystems, allowing easy key extraction even in cases where cryptanalysis attack would have been impractical [21], [22]. FIAs on Deep Neural Networks (DNNs) represent a critical security threat where an adversary manipulates the model's output by inducing transient or permanent errors in the underlying hardware [23]. In the context of edge AI, these attacks typically target the model weights stored in memory [14] or the activations during runtime computation [24], [25]. Such corruptions allow several different attack vectors:

- Misclassification: the basic attack, referred to as “evasion” in the context of adversarial learning. It can either be untargeted [14] or targeted [26], meaning that the attacker either achieves a random class output or a specific class output.

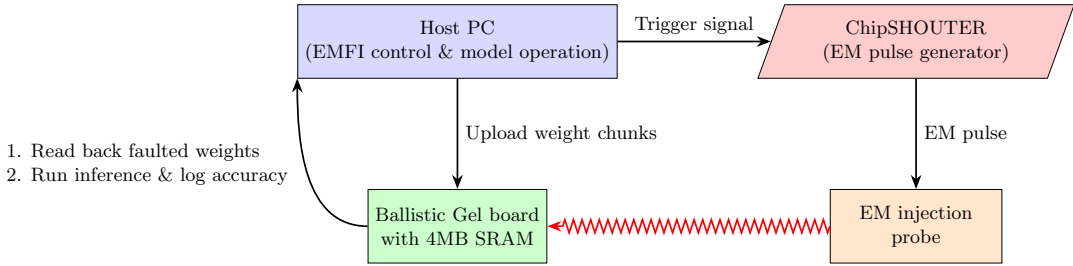


Fig. 2. Experimental electromagnetic fault injection setup overview.

- Reverse engineering: also referred to as “model stealing/extraction.” It was shown that precisely controlled bit flips can precisely recover model parameters [15].
- Backdoor/trojan planting: in this attack, the attacker either plants the backdoor during the training [27], [28] or after the model deployment [29]. Then, a specific trigger inserted in the network input causes the model misbehavior.

Additionally, fault attacks can cause a generic denial of service attack by making the system unresponsive, but this attack vector is not specific to neural networks and can generally be achieved by simpler means in practice (e.g., by making the power source unavailable).

#### D. Electromagnetic Fault Injection

Electromagnetic fault injection (EMFI) is a non-invasive physical attack technique used to disrupt the normal execution of an integrated circuit (IC) by inducing localized transient faults [30]. Unlike contact-based methods such as clock or voltage glitching, EMFI utilizes Faraday’s Law of Induction to create internal currents without physical modification of the target package. While it can be more precise if the IC package is opened, faults can still be triggered through the package, making it one of the biggest advantages over the laser fault injection [31], along with the equipment cost [3].

The core principle of EMFI involves a high-voltage pulse generator connected to an injection probe, typically consisting of a copper coil wound around a ferrite or mu-metal core [32]. When a rapid current pulse passes through the coil, it generates a time-varying magnetic field  $\vec{B}(t)$ . According to Faraday’s Law (see, for example, [33]), the electromotive force (EMF) induced in the underlying silicon circuitry is given by:

$$\mathcal{E} = -\frac{d\Phi_B}{dt} = -\frac{d}{dt} \int \vec{B} \cdot d\vec{A} \quad (4)$$

where  $\Phi_B$  is the magnetic flux passing through the sensitive loops of the IC’s metal layers. This induced voltage can momentarily exceed the threshold voltages of transistors or disrupt the propagation of signals along data buses, leading to bit-flips in registers, memory cells, or instruction flow errors [4].

The efficacy of an EMFI attack is primarily governed by the rise time, pulse width, and peak voltage of the injection signal. In our setup, we utilize a high-voltage pulse generator (NewAE ChipSHOUTER) capable of generating transient pulses with a magnitude of 200-500V.

**Injection probes.** The injection probe acts as the transducer that converts the electrical pulse into a localized magnetic field. Our study utilizes a micro-probe designed for high-precision spatial targeting.

The following properties influence the success and the precision of the EMFI attack [34]:

- Core material: the probe utilizes a high-permeability ferrite core. The ferrite material serves to concentrate the magnetic flux lines, minimizing far-field interference and ensuring that the fault is localized to a specific region of the SoC (e.g., the SRAM block or the instruction pipeline).
- Coil topology: the probe consists of several turns (typically 5–20) of fine copper wire. A lower number of turns reduces the total inductance, allowing for faster rise times, whereas a higher number of turns increases the peak magnetic field strength at the cost of temporal resolution.
- Probe tip geometry: the probe tip determines the shape and the size of the electromagnetic field generated by the probe. We use a relatively large tip with a diameter of 4 mm, allowing us to target multiple memory banks at the same time.

To characterize the vulnerability of the target, the probe is normally mounted on a high-precision XYZ motorized stage. By automating the displacement of the probe across the surface of the IC, a “fault map” can be generated for further analysis. In our case, the mapping process was synchronized with the trigger signal of the DNN inference, ensuring that the pulse was injected during the exact window when the weights of the targeted layers were stored in the memory.

## IV. EVALUATION METHOD

In this section, we first present the experimental setup in Subsection IV-A, followed by a discussion of the surface scan results, which identify the most vulnerable region of the chip, in Subsection IV-B.

### A. Experimental Setup

The components of the experimental setup along with their function are depicted in Fig. 2. The core of the setup consists of the electromagnetic fault injection device NewAE ChipSHOUTER<sup>1</sup>. An important component of the EMFI setup

<sup>1</sup><https://chipwhisperer.readthedocs.io/en/latest/ChipSHOUTER/ChipSHOUTER.html>



Fig. 3. NewAE ChipSHOUTER EMFI device mounted on the Ender-3 3D printer used as a positioning device. The Ballistic Gel board with the 4MB SRAM chip used as the DUT is positioned below the ChipSHOUTER.

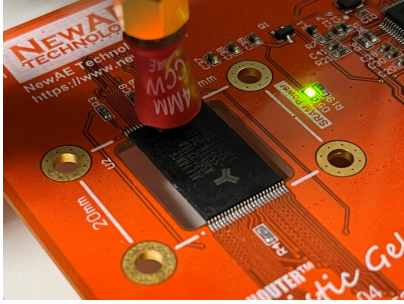


Fig. 4. Detail of the EM probe above the SRAM chip.

is the injection probe. We used a 4mm probe with a counter-clockwise wiring around its ferrite core (see Fig. 4 for the detail). With this device, we targeted the CW521 Ballistic Gel, which is a board hosting a 4MB SRAM chip AS6C3216A-55TIN from manufacturer ALLIANCE MEMORY based on CMOS technology. In the later text, we refer to this board as the DUT (device under test). The Ender-3 V3 SE 3D printer was used as an XYZ positioning device with a modification, where the printhead was replaced with a ChipSHOUTER mounted on a 3D printed holder. The fault injection bench is depicted in Fig. 3. The controlling of the ChipSHOUTER and the positioning device, communication with the DUT, and all the operations related to the neural network model were done on the Host PC.

After the initial evaluation, we arrived at a set of fault injection parameters that successfully produced faults in the memory. We used a voltage of 300V and a single pulse with the width of 160ns. During the attack, an electromagnetic pulse was generated only once.

### B. Surface Scan

To find the best probe position to trigger faults, we did an initial surface scan of the chip. The AS6C3216A-55TIN is packaged in a TSOP I surface-mount package of size  $12 \times$

$20 \text{ mm}^2$ . Z-axis was fixed and set to be 1 mm above the chip surface. We used 20 points in X direction and 40 points in Y direction ( $\approx 0.5 \text{ mm}$  step size), resulting to 800-point scan. For each point, we uploaded random bytes to fill the entire SRAM and did the electromagnetic fault injection. After the attack, we downloaded the data from the chip and compared it with the original data to check the proportion of corrupted bytes – our success rate. This is depicted in Fig. 5. We can see that the sweet spot is around the coordinate (7, 35), with  $\approx 15\%$  success rate. The position of the probe above this spot is shown in Fig. 4.

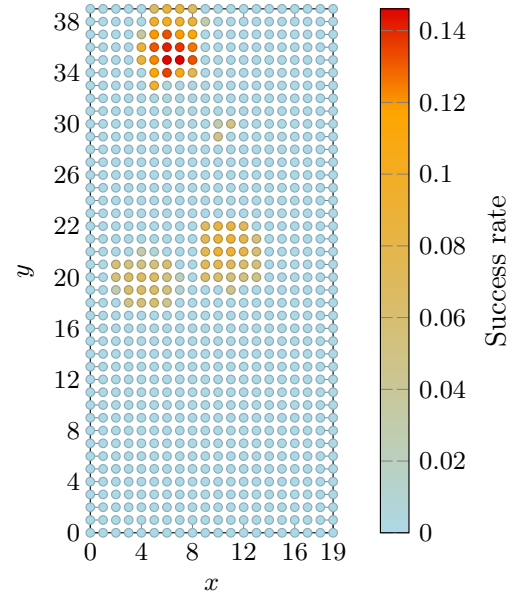


Fig. 5. Surface scan showing the success rate per point – proportion of corrupted bytes in the SRAM.

## V. EXPERIMENTAL RESULTS

To evaluate the impact of EMFI on model integrity, we employed the ImageNet-1K validation dataset, sub-sampled to 4,096 images using a fixed seed (21) for reproducibility. ImageNet-1K images are divided into 1,000 classes; the random guess accuracy corresponds to 0.1%. Inference was performed using the ONNX Runtime with CUDA acceleration on an NVIDIA RTX 4080 SUPER. We measured the degradation of model performance using Top-1 and Top-5 accuracy across four weight representations: FP32, FP16, INT8, and INT4. Vanilla accuracies across all the evaluated models are stated in Table III.

Next, we present the results on the impact of EMFI on data stored in memory in Subsection V-A. We then report the model accuracies after EMFI for different neural network architectures and weight representations in Subsection V-B. Finally, we discuss potential reasons for the observed disparity in resilience between floating-point and integer representations.

### A. Characterization of the EMFI Error Pattern

To quantify the impact of EMFI on the target's memory subsystem, we first characterized the fault effects on a linear

TABLE III  
VANILLA TOP-1 AND TOP-5 ACCURACY (%) FOR EVALUATED ARCHITECTURES IN THE UNATTACKED STATE ACROSS FOUR WEIGHT REPRESENTATIONS.

Model	Type	Top-1 (%)	Top-5 (%)
ResNet18	FP32	68.750	88.379
	FP16	68.774	88.379
	INT8	68.774	88.452
	INT4	67.236	87.549
ResNet34	FP32	72.778	90.991
	FP16	72.803	90.967
	INT8	72.583	90.942
	INT4	71.973	90.308
ResNet50	FP32	75.562	92.456
	FP16	75.513	92.481
	INT8	75.244	92.334
	INT4	74.683	91.821
VGG11	FP32	68.311	88.623
	FP16	68.335	88.599
	INT8	68.189	88.648
	INT4	68.164	88.062

data buffer. By applying a bitwise XOR operation between the original and post-attack data, we mapped the distribution of corrupted bits across the logical address space.

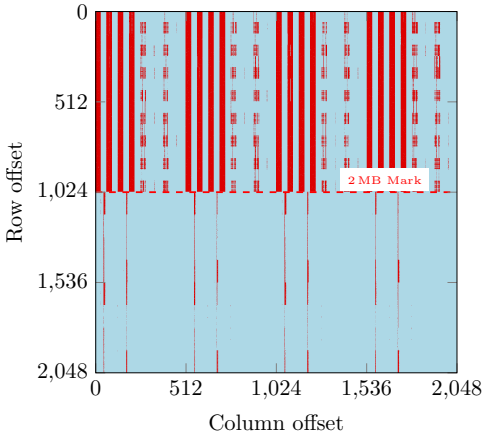


Fig. 6. Logical memory map of EMFI effects on a 4MB weight buffer. Red color indicates memory corruption. A significant decrease in fault density is observed after the 2MB offset, suggesting a boundary transition in the memory controller's handling of burst data or physical proximity limits of the EM probe.

As shown in Fig. 6, the faults exhibit a distinct periodicity. While we visualize this as a 2D matrix to identify recurring structures, it is important to note that this represents a linear sequence of addresses rather than the physical topology of the RAM cells. A significant transition was observed at the 2MB offset:

- **0–2MB region:** high density of periodic corruption, suggesting a specific interaction between the EM pulse and the memory controller's burst-access logic or internal buffering.
- **Post-2MB region:** a sharp decline in fault density, which may indicate a boundary in the memory allocation or a

physical distance limit of the EM probe's effective field relative to the underlying chip.

This pattern proved highly deterministic, persisting across power cycles and multiple days of testing. This repeatability suggests that the vulnerability is not a stochastic "white noise" effect but is tied to the architectural handling of data at specific logical offsets.

### B. Sensitivity Analysis across Architectures

We conducted a granular sensitivity analysis by replacing 4MB segments of model parameters. A total of 352 unique fault-injected models were evaluated. An overview of results on evaluated architectures and weight representations is provided in Fig. 7.

Table IV provides a consolidated overview of the spatial sensitivity analysis across selected evaluated ResNet and VGG architectures. We omitted the rest of the architectures as the after-attack accuracies for all the attacked chunks were too low to draw any conclusions. Here, chunks are defined as contiguous 4MB segments of the model's weight tensors, which were individually replaced during our fault-injection experiments to isolate local vulnerabilities. The table summarizes the total chunk count for each model and data type configuration, alongside the resulting Top-1 accuracy when targeting specific spatial regions: the Front (initial layers), the Middle (intermediate layers), and the Back (final layers/fully connected layers).

1) *ResNet Analysis:* The ResNet architecture (ResNet18, 34, 50) exhibited extreme sensitivity to EMFI when using floating-point representations.

The following observations can be made:

- **Floating-point (FP32/FP16):** in all tested cases, the Top-1 and Top-5 accuracy dropped close to a random guess, indicating a total collapse of the model's predictive capability (Fig. 7 (a), (b)).
- **Integer (INT8/INT4):** while these models suffered significant accuracy degradation, they did not drop to a random guess in all the cases (Fig. 7 (c), (d)).
- **Spatial sensitivity :** we observed a "front-heavy" sensitivity profile for networks listed in Table IV. Faults injected into the initial convolutional layers resulted in massive accuracy drops, whereas layers toward the end of the network (e.g., fully connected layers) exhibited higher resilience.

2) *VGG Analysis:* The VGG architecture demonstrated distinct failure modes compared to ResNet. While FP32 models collapsed to a near-random guess accuracy, the FP16 VGG variants showed localized resilience; for instance, replacing the final 1.4 MB chunk resulted in a Top-1 accuracy of ~63% (Table IV).

Furthermore, the INT8 and INT4 quantized VGG models displayed a bi-modal sensitivity profile – attacking the first and the last layers led to heavy accuracy drops, while attacking the middle layers kept it at a vanilla level. Significant accuracy loss was primarily localized to the replacement of the first and last parameter chunks, while the intermediate layers remained largely unaffected, maintaining performance levels near the pre-attack baseline.

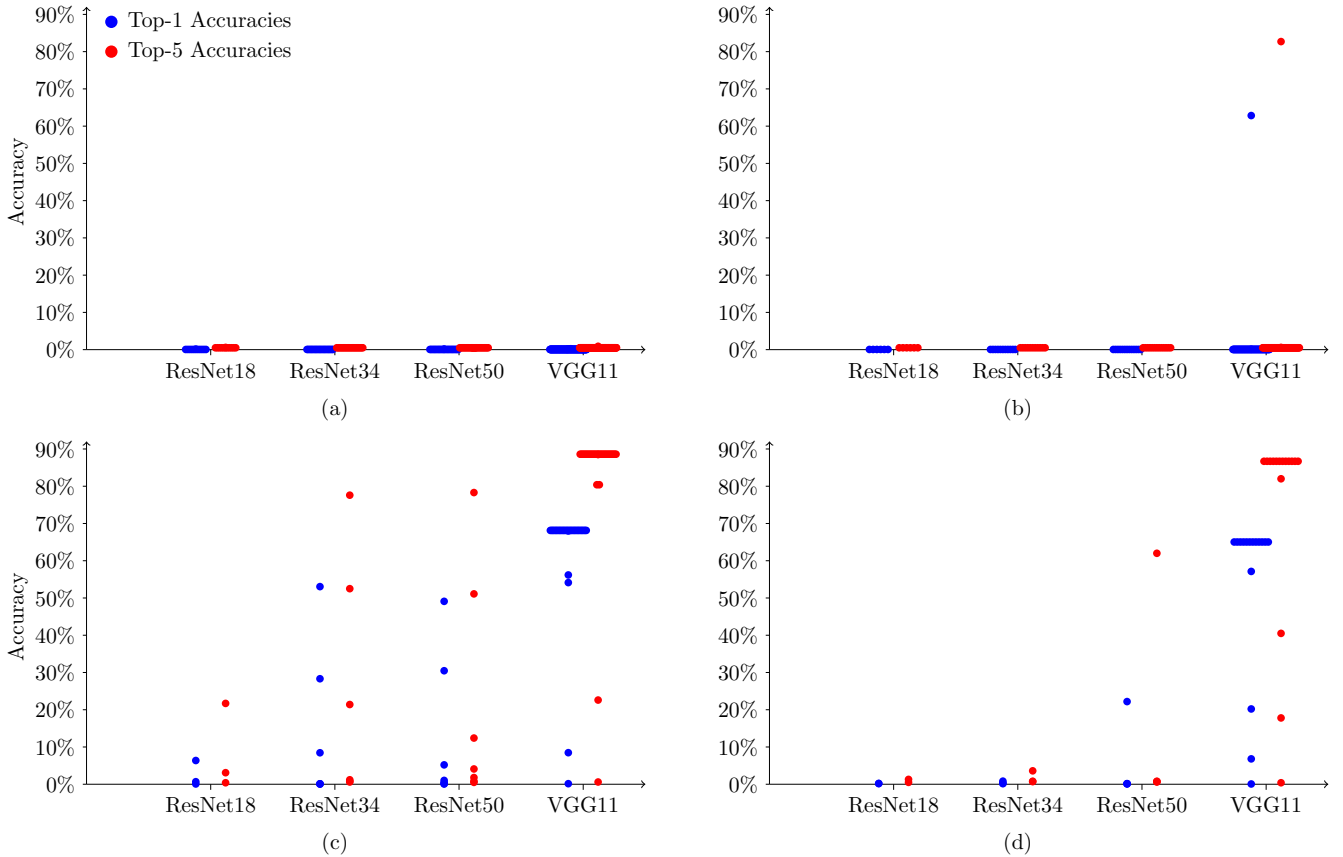


Fig. 7. Classification accuracy under fault injection for ResNet-18, ResNet-34, ResNet-50, and VGG-11. Each marker corresponds to the top-1 (blue) or top-5 (red) accuracy obtained after injecting faults into a specific chunk of the model’s weight parameters. Results are reported for four weight representations: (a) FP32, (b) FP16, (c) INT8, and (d) INT4.

TABLE IV

CONSOLIDATED SPATIAL SENSITIVITY: TARGETED CHUNK ACCURACY (TOP-1 %). FRONT/MIDDLE/BACK DENOTE IN WHICH PART OF THE NETWORK THE ATTACK HAPPENED. TARGETING THE CHUNKS AT THE BEGINNING (FRONT) ALWAYS LEADS TO A COMPLETE ACCURACY DEGRADATION.

Model	Type	# Chunks	Front	Middle	Back
ResNet18	INT8	3	0.07%	0.68%	6.37%
ResNet34	INT8	6	0.10%	0.12%	53.05%
ResNet50	INT8	7	0.15%	5.20%	49.10%
ResNet50	INT4	4	0.12%	0.17%	22.19%
VGG11	FP32	127	0.05%	0.05%	0.12%
VGG11	FP16	64	0.05%	0.05%	62.84%
VGG11	INT8	32	0.15%	68.14%	54.13%
VGG11	INT4	16	0.07%	65.03%	20.21%

### C. Impact of Data Representation on Fault Severity

The disparity between floating-point and integer resilience can be attributed to the underlying bit-level numerical representations and how they handle corruption:

- 1) **Floating-point instability:** binary analysis reveals that EMFI in this specific setup frequently results in bytes being set to 0xFF or 0xFE (see Fig. 8). In the IEEE 754 standard (FP32), a sequence of 0xFF often leads to **NaN (Not a Number)** or values exceeding the representable range. We observed the weight range of

a ResNet18 chunk shift from  $[-1.04, 0.76]$  to approximately  $[-3.4 \times 10^{38}, 3.3 \times 10^{38}]$  post-injection. A single such extremal value can propagate through the network’s activation functions, effectively “poisoning” the entire feature map.

- 2) **Integer robustness:** in contrast, INT8 and INT4 representations are strictly bounded by their bit-width (ranges of  $[-128, 127]$  and  $[-8, 7]$ , respectively). Even a worst-case bit flip cannot cause the exponential magnitude shift observed in floating-point formats, thereby preventing the catastrophic propagation of NaN-like values.

To summarize, the results suggest that INT8 quantization offers the optimal balance between inference accuracy and EMFI resilience for edge deployments. Beyond reduced memory footprints, the bounded nature of integer arithmetic provides an inherent layer of “numerical masking” against the high-magnitude bit-flips typical of EMFI attacks.

## VI. DISCUSSION

**Number representations and fault tolerance.** As explained in the previous part, the difference in fault resilience between floating-point and integer representations is not just a matter of bit-width, but is fundamentally rooted in the dynamic

Address	00	01	02	03	04	05	06	07	08	09	0A	0B	0C	0D	0E	0F	ASCII
00000000:	A4	70	47	3B	7D	50	5B	3B	71	98	65	BB	63	B7	AB	BB	.pG;)P{q.e...
00000010:	41	EA	18	BC	3B	E8	20	BC	8A	47	84	BC	81	83	76	3A	.A..8.. .G..v:
00000020:	E3	EB	AE	3A	BE	90	5F	3B	29	FE	99	3B	3D	FA	03	3A	.....;)=.=.:
00000030:	15	63	9C	BC	CF	04	10	BC	80	FE	A6	3B	26	72	B0	3B	.c.....;kz.;
00000040:	30	19	71	3B	58	09	5C	3C	35	C0	3C	EE	38	6A	3C	0.q;X..5..C..8..j<	
00000050:	BA	58	42	3C	B7	88	AD	3B	5F	DC	79	3A	7C	AC	2B	BC	X.Bc...;jy!..+
00000060:	83	36	36	BC	40	5A	75	BB	DB	72	16	3C	64	1A	76	3C	.66.0zU..r..d..v<
00000070:	1D	35	58	B9	6A	A6	CF	3B	4A	23	17	BB	18	22	4F	BC	.5X.j..;J#..".0.
00000080:	BF	D6	ED	BC	32	37	8F	BC	0E	AC	EA	3A	97	BC	56	3A	.27.....;V:
00000090:	4F	7E	33	3C	B9	03	68	3C	33	D4	9D	3C	F5	78	B5	3B	0.3X..h3K..x..<
000000A0:	D7	BB	FB	BB	E2	F2	6A	BB	5C	9E	95	BC	EA	15	F1	BB	.....;j.....
000000B0:	33	2B	85	BB	15	88	FF	3B	F6	35	04	3C	25	CD	A7	3B	3+.....;5.<%..;
000000C0:	8D	53	CC	39	C6	FC	89	BB	91	B9	2A	3B	70	5B	B2	3B	.S.9.....;pL;
000000D0:	3C	1F	4E	3C	66	EC	48	3C	E9	99	24	3C	7B	99	0D	BB	<.N<E.H..S<{...
000000E0:	E9	24	E7	BA	3A	43	8D	3B	20	30	7E	3C	OE	F4	3C	\$.C.; 0<<..<	
000000F0:	C7	26	15	3D	B9	88	08	3D	AC	51	E0	3C	22	OC	2C	BC	.&.=.=.Q..<".

Address	00	01	02	03	04	05	06	07	08	09	0A	0B	0C	0D	0E	0F	ASCII
00000000:	FE	.<.....															
00000010:	00	3C	.<.<.<.<.<.<.<														
00000020:	E3	EB	AE	3A	EE	90	5F	3B	29	FE	99	3B	3D	FA	03	3A	. ....;)=.:
00000030:	15	63	9C	BC	CF	04	10	BC	80	FE	A6	3B	26	72	B0	3B	.c.....;kz.;
00000040:	30	19	71	3B	58	09	5C	3C	35	C0	3C	EE	38	6A	3C	0.q;X..5..C..8..j<	
00000050:	BA	58	42	3C	B7	88	AD	3B	5F	DC	79	3A	7C	AC	2B	BC	X.Bc...;jy!..+
00000060:	83	36	36	BC	40	5A	75	BB	DB	72	16	3C	64	1A	76	3C	.66.0zU..r..d..v<
00000070:	1D	35	58	B9	6A	A6	CF	3B	4A	23	17	BB	18	22	4F	BC	.5X.j..;J#..".0.
00000080:	BF	D6	ED	BC	32	37	8F	BC	0E	AC	EA	3A	97	BC	56	3A	.27.....;V:
00000090:	4F	7E	33	3C	B9	03	68	3C	33	D4	9D	3C	F5	78	B5	3B	0.3X..h3K..x..<
000000A0:	D7	BB	FB	BB	E2	F2	6A	BB	5C	9E	95	BC	EA	15	F1	BB	.....;j.....
000000B0:	33	2B	85	BB	15	88	FF	3B	F6	35	04	3C	25	CD	A7	3B	3+.....;5.<%..;
000000C0:	8D	53	CC	39	C6	FC	89	BB	91	B9	2A	3B	70	5B	B2	3B	.S.9.....;pL;
000000D0:	3C	1F	4E	3C	66	EC	48	3C	E9	99	24	3C	7B	99	0D	BB	<.N<E.H..S<{...
000000E0:	E9	24	E7	BA	3A	43	8D	3B	20	30	7E	3C	OE	F4	3C	\$.C.; 0<<..<	
000000F0:	C7	26	15	3D	B9	88	08	3D	AC	51	E0	3C	22	OC	2C	BC	.&.=.=.Q..<".

Fig. 8. Binary comparison of data before the attack (left) and after the attack (right)

range and the non-linear mapping of the IEEE 754 floating-point standard compared to constant resolution scaling for integers. Apart from that, a phenomena of activation function saturation appears in floating-point models:

- In FP32, a post-attack weight of  $10^{38}$  will result in an activation value so large that it either leads to numerical overflow in the next layer or permanently “saturates” the neuron.
- In quantized networks, weights and activations are usually clipped or normalized. Even if a weight is flipped to its maximum integer value, the scaling factors used in INT8/4 quantization act as a natural shock absorber, preventing a single bit-flip from dominating the entire feature map.

**Embedded memory limit.** One potential limitation of our experimental platform is the 4 MB memory capacity, which is modest compared to contemporary high-performance AI accelerators. However, this choice was deliberate and aligned with the objectives of this study. Our goal is not to evaluate absolute fault rates in highly optimized systems, but rather to characterize and compare the intrinsic sensitivity of different numerical representations used in neural network weights.

Highly integrated SoCs typically employ memory interleaving, redundancy, and hardware-level error correction mechanisms, which introduce confounding factors that can obscure the direct relationship between injected faults and their algorithmic impact. By using a linear, non-interleaved memory architecture without error correction codes, we are able to isolate the mathematical propagation of memory faults within the network and study representation-dependent effects in a controlled and reproducible manner.

Moreover, this memory scale is representative of the emerging Micro-AI and edge-inference domain, where resource-constrained microcontrollers deploy neural networks in safety- and security-critical applications. In this context, understanding the fundamental resilience of numerical representations is particularly relevant.

We note that extending this analysis to large-scale accelerators with complex memory hierarchies is an important direction for future work; however, such platforms would primarily affect the fault injection surface rather than the representation-level vulnerability analyzed in this paper.

**Countermeasures.** Countermeasures against fault injection attacks are a well-studied topic in the realm of cryptogra-

phy [35]. Some methods can be directly used to protect embedded neural networks, such as detection circuits [36], [37] and error correcting/detecting codes [38]–[40]. Apart from that, there are specific methods that were developed for protecting deep learning, we state the most prominent approaches below. A method called DeepDyve [41] utilizes small, pre-trained neural networks to verify the outputs of the main model. RADAR [42] protection stores a 2-bit checksum for a group of weights in memory during the deployment and then checks the integrity of the weights at runtime. The detection rate is 96.1% with  $\approx 1\%$  computational overhead and 5.6 KB of memory overhead for ResNet-18. HASHTAG [43] also focuses on detection, but using cryptographic hashing instead of simple checksums. ALERT [44] monitors and detects abnormal neuron activation patterns that are caused by faults. When such anomalies are triggered, ALERT activates a recovery mechanism to mitigate the impact of the attack.

## VII. CONCLUSION

In this work, we have presented a comprehensive analysis of EMFI on embedded neural networks to study the influence of different number representations on model resistance against the attack.

We demonstrated that the numerical representation of weights is a significant factor in model resilience: while floating-point models suffer from catastrophic accuracy collapse due to NaN propagation and exponent bit-flips, quantized models provide inherent defense through numerical clipping.

As a potential future direction, it would be worthwhile to study training phase possibilities towards fault resistance. While INT8 provides passive protection, new quantization-aware training schemes could be developed to specifically minimize the bit-error sensitivity of the most influential weight bits.

**Acknowledgement:** OpenAI ChatGPT and Google Gemini LLMs were used to improve clarity and readability of some portions of this manuscript.

## REFERENCES

- [1] J. Lin, L. Zhu, W.-M. Chen, W.-C. Wang, and S. Han, “Tiny machine learning: Progress and futures [feature],” *IEEE Circuits and Systems Magazine*, vol. 23, no. 3, pp. 8–34, 2023.
- [2] T. Liang, J. Glossner, L. Wang, S. Shi, and X. Zhang, “Pruning and quantization for deep neural network acceleration: A survey,” *Neurocomputing*, vol. 461, pp. 370–403, 2021.

- [3] J. Breier and X. Hou, "How practical are fault injection attacks, really?" *IEEE Access*, vol. 10, pp. 113 122–113 130, 2022.
- [4] M. Dumont, M. Lisart, and P. Maurine, "Electromagnetic fault injection: How faults occur," in *2019 Workshop on Fault Diagnosis and Tolerance in Cryptography (FDTC)*. IEEE, 2019, pp. 9–16.
- [5] B. Goswami, R. Chetry, C. Moorthii J. and M. Suri, "Investigation of em fault injection on emerging lightweight neural network hardware," in *International Conference on Applied Cryptography and Network Security*. Springer, 2025, pp. 113–123.
- [6] S. Hashemi, N. Anthony, H. Tann, R. I. Bahar, and S. Reda, "Understanding the impact of precision quantization on the accuracy and energy of neural networks," in *Design, Automation & Test in Europe Conference & Exhibition (DATE)*, 2017. IEEE, 2017, pp. 1474–1479.
- [7] M. Nagel, M. Fournarakis, R. A. Amjad, Y. Bondarenko, M. Van Baalen, and T. Blankevoort, "A white paper on neural network quantization," *arXiv preprint arXiv:2106.08295*, 2021.
- [8] W. Guillemé, A. Kritikakou, Y. Helen, C. Killian, and D. Chillet, "Fault tolerance in quantized and pruned convolutional neural networks," in *IEEE International Symposium on On-Line Testing and Robust System Design (IOLTS)*, 2025, pp. 1–7.
- [9] S. Hong, P. Frigo, Y. Kaya, C. Giuffrida, and T. Dumitras, "Terminal brain damage: Exposing the graceless degradation in deep neural networks under hardware fault attacks," in *28th USENIX Security Symposium (USENIX Security 19)*, 2019, pp. 497–514.
- [10] B. Goswami, R. Chetry, C. Moorthii, and M. Suri, "Investigation of em fault injection on emerging lightweight neural network hardware," in *Applied Cryptography and Network Security Workshops (ACNS)*. Springer, 2025, pp. 113–123.
- [11] K. He, X. Zhang, S. Ren, and J. Sun, "Deep residual learning for image recognition," in *Proceedings of the IEEE conference on computer vision and pattern recognition (CVPR)*, 2016, pp. 770–778.
- [12] K. Simonyan and A. Zisserman, "Very deep convolutional networks for large-scale image recognition," *arXiv preprint arXiv:1409.1556*, 2014.
- [13] J. Deng, W. Dong, R. Socher, L.-J. Li, K. Li, and L. Fei-Fei, "Imagenet: A large-scale hierarchical image database," in *2009 IEEE conference on computer vision and pattern recognition*. Ieee, 2009, pp. 248–255.
- [14] A. S. Rakin, Z. He, and D. Fan, "Bit-flip attack: Crushing neural network with progressive bit search," in *Proceedings of the IEEE/CVF International Conference on Computer Vision*, 2019, pp. 1211–1220.
- [15] J. Breier, D. Jap, X. Hou, S. Bhasin, and Y. Liu, "Sniff: Reverse engineering of neural networks with fault attacks," *IEEE Transactions on Reliability*, vol. PP, no. 99, pp. 1–13, 2021.
- [16] F. Libano, B. Wilson, M. Wirthlin, P. Rech, and J. Brunhaver, "Understanding the impact of quantization, accuracy, and radiation on the reliability of convolutional neural networks on fpgas," *IEEE Transactions on Nuclear Science*, vol. 67, no. 7, pp. 1402–1410, 2020.
- [17] C. Gaine, P.-A. Moëllic, O. Potin, and J.-M. Dutertre, "Fault injection on embedded neural networks: Impact of a single instruction skip," in *IEEE Euromicro Conference on Digital System Design (DSD)*, 2023, preprint accepted at DSD2023, AHSA Special Session.
- [18] N. N. Alajlan and D. M. Ibrahim, "Tinyml: Enabling of inference deep learning models on ultra-low-power iot edge devices for ai applications," *Micromachines*, vol. 13, no. 6, p. 851, 2022.
- [19] R. David, J. Duke, A. Jain, V. Janapa Reddi, N. Jeffries, J. Li, N. Kreeger, I. Nappier, M. Natraj, T. Wang *et al.*, "Tensorflow lite micro: Embedded machine learning for tinyml systems," *Proceedings of machine learning and systems*, vol. 3, pp. 800–811, 2021.
- [20] B. Parhami, *Computer arithmetic*. Oxford university press Oxford, 1999, vol. 20, no. 00.
- [21] D. Boneh, R. A. DeMillo, and R. J. Lipton, "On the importance of checking cryptographic protocols for faults," in *Advances in Cryptology—EUROCRYPT'97: International Conference on the Theory and Application of Cryptographic Techniques Konstanz, Germany, May 11–15, 1997 Proceedings*. Springer, 1997, pp. 37–51.
- [22] J. Breier, X. Hou, and S. Bhasin, *Automated Methods in Cryptographic Fault Analysis*. Springer, 2019.
- [23] Y. Liu *et al.*, "Fault injection attacks on deep neural networks: Lessons learned," in *Design Automation Conference (DAC)*, 2017.
- [24] X. Hou, J. Breier, D. Jap, L. Ma, S. Bhasin, and Y. Liu, "Physical security of deep learning on edge devices: Comprehensive evaluation of fault injection attack vectors," *Microelectronics Reliability*, vol. 120, p. 114116, 2021.
- [25] J. Breier, X. Hou, D. Jap, L. Ma, S. Bhasin, and Y. Liu, "Practical fault attack on deep neural networks," in *Proceedings of the 2018 ACM SIGSAC Conference on Computer and Communications Security*, 2018, pp. 2204–2206.
- [26] A. S. Rakin, Z. He, J. Li, F. Yao, C. Chakrabarti, and D. Fan, "T-bfa: Targeted bit-flip adversarial weight attack," *IEEE Transactions on Pattern Analysis and Machine Intelligence*, vol. 44, no. 11, pp. 7928–7939, 2021.
- [27] J. Breier, X. Hou, M. Ochoa, and J. Solano, "Foobar: Fault fooling backdoor attack on neural network training," *IEEE Transactions on Dependable and Secure Computing*, vol. 20, no. 3, pp. 1895–1908, 2022.
- [28] C. Martínez-Mejía, J. Solano, J. Breier, D. Bucko, and X. Hou, "Deepbar: Fault backdoor attack on deep neural network layers," *arXiv preprint arXiv:2407.21220*, 2024.
- [29] A. S. Rakin, Z. He, and D. Fan, "Tbt: Targeted neural network attack with bit trojan," in *Proceedings of the IEEE/CVF conference on computer vision and pattern recognition*, 2020, pp. 13 198–13 207.
- [30] S. Habibi and et al., "Emfi: Electromagnetic fault injection on microcontrollers," in *International Conference on Security and Cryptography (SECRYPT)*, 2021.
- [31] J. Breier and D. Jap, "Testing feasibility of back-side laser fault injection on a microcontroller," in *Proceedings of the WESS'15: Workshop on Embedded Systems Security*, 2015, pp. 1–6.
- [32] X. Hou and J. Breier, *Cryptography and Embedded Systems Security*. Springer, 2024.
- [33] K. Kuehn, "Faraday's law," in *A Student's Guide Through the Great Physics Texts: Volume III: Electricity, Magnetism and Light*. Springer, 2015, pp. 331–344.
- [34] C. Gaine, J.-P. Nikolovski, D. Aboulkassimi, and J.-M. Dutertre, "New probe design for hardware characterization by electromagnetic fault injection," in *2022 International Symposium on Electromagnetic Compatibility—EMC Europe*. IEEE, 2022, pp. 299–304.
- [35] A. Baksi, S. Bhasin, J. Breier, D. Jap, and D. Saha, "A survey on fault attacks on symmetric key cryptosystems," *ACM Computing Surveys*, vol. 55, no. 4, pp. 1–34, 2022.
- [36] L. Zussa, A. Dehbaoui, K. Tobich, J.-M. Dutertre, P. Maurine, L. Guillaume-Sage, J. Clediere, and A. Tria, "Efficiency of a glitch detector against electromagnetic fault injection," in *2014 Design, Automation & Test in Europe Conference & Exhibition (DATE)*. IEEE, 2014, pp. 1–6.
- [37] J. Breier, S. Bhasin, and W. He, "An electromagnetic fault injection sensor using hogge phase-detector," in *2017 18th International Symposium on Quality Electronic Design (ISQED)*. IEEE, 2017, pp. 307–312.
- [38] X. Guo and R. Karri, "Recomputing with permuted operands: A concurrent error detection approach," *IEEE Transactions on Computer-Aided Design of Integrated Circuits and Systems*, vol. 32, no. 10, pp. 1595–1608, 2013.
- [39] J. Breier, X. Hou, and Y. Liu, "On evaluating fault resilient encoding schemes in software," *IEEE Transactions on Dependable and Secure Computing*, vol. 18, no. 3, pp. 1065–1079, 2019.
- [40] J. Breier, M. Khairallah, X. Hou, and Y. Liu, "A countermeasure against statistical ineffective fault analysis," *IEEE Transactions on Circuits and Systems II: Express Briefs*, vol. 67, no. 12, pp. 3322–3326, 2020.
- [41] Y. Li, M. Li, B. Luo, Y. Tian, and Q. Xu, "DeepDyve: Dynamic verification for deep neural networks," in *Proceedings of the 2020 ACM SIGSAC Conference on Computer and Communications Security*, 2020, pp. 101–112.
- [42] J. Li, A. S. Rakin, Z. He, D. Fan, and C. Chakrabarti, "Radar: Runtime adversarial weight attack detection and accuracy recovery," in *2021 Design, Automation & Test in Europe Conference & Exhibition (DATE)*. IEEE, 2021, pp. 790–795.
- [43] M. Javaheripi and F. Koushanfar, "Hashtag: Hash signatures for online detection of fault-injection attacks on deep neural networks," in *2021 IEEE/ACM International Conference On Computer Aided Design (ICCAD)*. IEEE, 2021, pp. 1–9.
- [44] X. Wei, X. Wang, Y. Yan, N. Jiang, and H. Yue, "Alert: A lightweight defense mechanism for enhancing dnn robustness against t-bfa," *Journal of Systems Architecture*, vol. 152, p. 103160, 2024.